

Analysis and Optimization of the MODIS Leaf Area Index Algorithm Retrievals Over Broadleaf Forests

Nikolay V. Shabanov, Dong Huang, Wenze Yang, Bin Tan, Yuri Knyazikhin, Ranga B. Myneni, Douglas E. Ahl, Stith T. Gower, Alfredo R. Huete, *Member, IEEE*, Luiz Eduardo O. C. Aragão, and Yosio Edemir Shimabukuro

Abstract—Broadleaf forest is a major type of Earth's land cover with the highest observable vegetation density. Retrievals of biophysical parameters, such as leaf area index (LAI), of broadleaf forests at global scale constitute a major challenge to modern remote sensing techniques in view of low sensitivity (saturation) of surface reflectances to such parameters over dense vegetation. The goal of the performed research is to demonstrate physical principles of LAI retrievals over broadleaf forests with the Moderate Resolution Imaging Spectroradiometer (MODIS) LAI algorithm and to establish a basis for algorithm refinement. To sample natural variability in biophysical parameters of broadleaf forests, we selected MODIS data subsets covering deciduous broadleaf forests of the eastern part of North America and evergreen broadleaf forests of Amazonia. The analysis of an annual course of the Terra MODIS Collection 4 LAI product over broadleaf forests indicated a low portion of best quality main radiative transfer-based algorithm retrievals and dominance of low-reliable backup algorithm retrievals during the growing season. We found that this retrieval anomaly was due to an inconsistency between simulated and MODIS surface reflectances. LAI retrievals over dense vegetation are mostly performed over a compact location in the spectral space of saturated surface reflectances, which need to be accurately modeled. New simulations were performed with the stochastic radiative transfer model, which poses high numerical accuracy at the condition of saturation. Separate sets of parameters of the LAI algorithm were generated for deciduous and evergreen broadleaf forests to account for the differences in the corresponding surface reflectance properties. The optimized algorithm closely captures physics of seasonal variations in surface reflectances and delivers a majority of LAI retrievals during a phenological cycle, consistent with field measurements. The analysis of the optimized retrievals indicates that the precision of MODIS surface reflectances, the natural variability, and mixture of species set a limit to improvements of the accuracy of LAI retrievals over broadleaf forests.

Index Terms—Leaf area index (LAI), Moderate Resolution Imaging Spectroradiometer (MODIS), stochastic radiative transfer, surface reflectances, Terra.

Manuscript received April 4, 2004; revised March 30, 2005. This work was supported by the National Aeronautics and Space Administration under MODIS Contract NNG04HZ09C.

N. V. Shabanov, D. Huang, W. Yang, B. Tan, Y. Knyazikhin, and R. B. Myneni are with the Department of Geography, Boston University, Boston, MA 02215 USA (e-mail: shabanov@crsa.bu.edu).

D. E. Ahl and S. T. Gower are with the Department of Forest Ecology and Management, University of Wisconsin, Madison, WI 53706 USA.

A. Huete is with the Department of Soil, Water, and Environmental Science, University of Arizona, Tucson, AZ 85721 USA.

L. E. O. C. Aragão is with the School of Geography and the Environment, University of Oxford, Oxford, OX1 3TB, U.K. and also with the Instituto Nacional de Pesquisas Espaciais, Divisão de Sensoriamento Remoto, São José dos Campos, CEP 12227-010, C.P. 515, Brazil.

Y. E. Shimabukuro is with the Instituto Nacional de Pesquisas Espaciais, Divisão de Sensoriamento Remoto, São José dos Campos, CEP 12227-010, C.P. 515, Brazil.

Digital Object Identifier 10.1109/TGRS.2005.852477

I. INTRODUCTION

LEAF area index (LAI) is a key environmental variable controlling an exchange of fluxes of energy, mass (e.g., water and CO₂) and momentum between the Earth's surface and the atmosphere. LAI is defined as one-sided green leaf area per unit ground area in broadleaf canopies and as the projected needle leaf area in coniferous canopies. LAI is utilized in most ecosystem productivity models, global models of climate, hydrology, biogeochemistry, ecology, and multiple National Aeronautics and Space Administration (NASA) Earth Observing System (EOS) interdisciplinary projects [5], [7], [16], [19], [21], [22].¹

The Moderate Resolution Imaging Spectroradiometer (MODIS) onboard the EOS Terra and Aqua platforms delivers a set of remote sensing measurements to generate 11 MODIS Land (MODLAND) products, including LAI [10]. An algorithm for retrieval of LAI from MODIS surface reflectances was developed [12], [13] prototyped prior to the launch of MODIS with Advanced Very High Resolution Radiometer (AVHRR), Landsat Thematic Mapper (TM), Polarization and Directionality of the Earth's Reflectance (POLDER), and Sea-viewing Wide Field-of-view Sensor (SeaWiFS) data [28], [30], [36], and is in operational production [18].² Two versions of MODIS LAI products are currently available for public use: Collection 3 and, the latest, Collection 4.³ Current MODIS LAI research is focused on interdependent activities of product quality assessment [9], [26], [33], validation with field measurements [6], [17], [20], [27], [31], and algorithm refinement for future data reprocessing (Collection 5) (this paper).

Best quality LAI retrievals are performed with a main radiative transfer (RT)-based algorithm; in the case of its failure, poor-quality retrievals are generated by an empirical backup algorithm based on LAI and the normalized difference vegetation index (NDVI) [33]. Generally, two key factors influence the quality of retrievals by the MODIS LAI algorithm: 1) uncertainties in the input of the algorithm (surface reflectances and land cover); 2) model uncertainties, namely, the consistency between RT simulations, stored in the lookup tables (LUTs) of the algorithm, and the corresponding MODIS surface reflectances [9].

The analysis of the Collection 3 MODIS LAI product [33] and field measurements [34] indicates two major retrieval anomalies: LAI overestimation over certain areas with herbaceous vegetation, and dominance of poor-quality backup algorithm retrievals for woody vegetation during the growing season. The anomaly of the first type can be noted as nonphysical peaks

¹See also http://eosps0.gsfc.nasa.gov/science_plan/index.php.

²See also <http://edcdaac.usgs.gov/modis/mod15a2v4.asp>.

³See also <http://lpdaac.usgs.gov/modis/mod12q1v4.asp>.

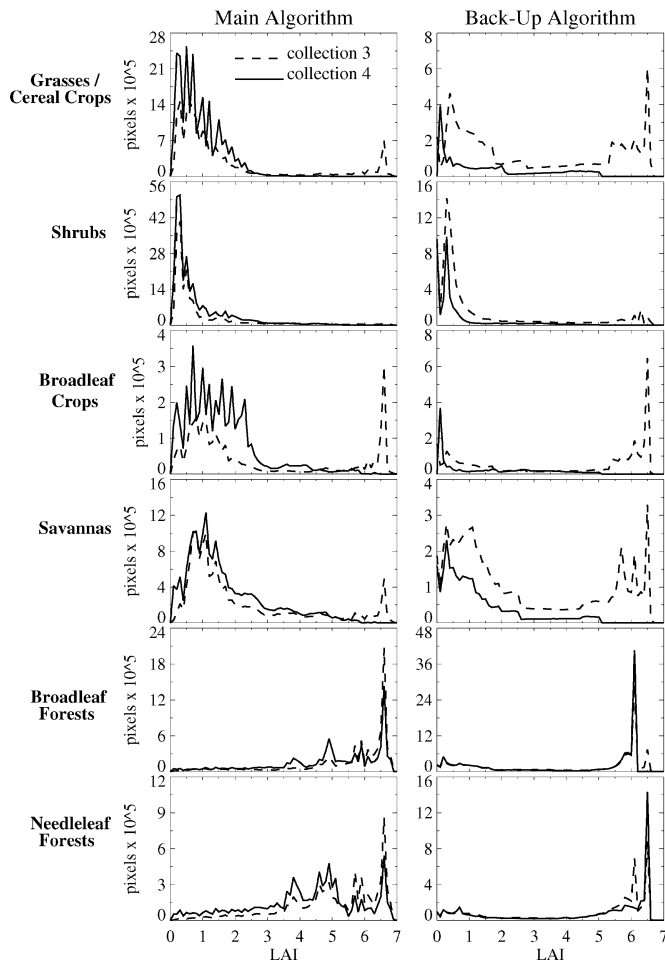


Fig. 1. Global histograms of the MODIS (dashed line) Collection 3 and (solid line) the Collection 4 LAI for Julian days 201–208 (July 20–27) in year 2001. Retrievals by the main and the backup algorithms are shown separately for six land cover types (biomes). Improvements in the algorithm and its inputs resulted in the correction of the unphysical peaks in LAI distributions at high values and the reduction of low reliable backup algorithm retrievals in the Collection 4 data for herbaceous vegetation (biomes 1–4).

at high LAI values at a global distribution of the Collection 3 product over herbaceous vegetation (Fig. 1). This anomaly was investigated and resolved in Collection 4 data reprocessing [9], [26], [33]. The anomaly of retrievals over woody vegetation is still present in the Collection 4 data. The causes of both anomalies will be detailed later in the text.

The goal of the presented research is to demonstrate the physical principles of LAI retrievals over broadleaf forests with the MODIS LAI algorithm, provide the basis for the Collection 5 algorithm refinement, and define the factors which set the upper limit on algorithm performance. The structure of this paper is as follows. Section II summarizes data on surface reflectances, land cover, and LAI from the Terra MODIS sensor, which were utilized in the analysis. Section III discusses the anomalies in the global LAI product for broadleaf forests. Section IV reviews the physical and mathematical basis of LAI retrievals with the MODIS LAI algorithm. Section V details LUT optimization for broadleaf forests. Section VI compares LAI derived with new LUTs, the Collection 4 LAI product, and field data. Section VII discusses the daily and seasonal variability of surface reflectances and the impact of uncertainties in surface reflectances on the accuracy of LAI retrievals.

II. DATA DESCRIPTION

This research utilizes three Terra MODIS Land products: LAI, surface reflectances, and land cover. We analyzed the Collection 4 Terra MODIS LAI product (MOD15A2). The MOD15A2 product is an eight-day compositing of daily LAI retrievals and provides LAI and corresponding quality controls variables (<http://edcdaac.usgs.gov/modis/mod15a2v4.asp>). Analysis and optimization of MODIS LAI retrievals was performed on the basis of the Collection 4 Terra MODIS daily aggregated surface reflectances (MODAGAGG product). The MODAGAGG product includes atmospherically corrected surface reflectance in seven spectral bands, viewing and illumination angles, and quality control variables [29]. To mask vegetation type of interest (broadleaf forests) we referenced the Collection 3 Terra MODIS land cover (MOD12Q1 product) [8], which was used to generate the Collection 4 LAI data. The MOD12Q1 product provides a six-biome classification scheme: 1) grasses and cereal crops; 2) shrubs; 3) broadleaf crops; 4) savannas; 5) broadleaf forests; and 6) needle leaf forests (<http://lpdaac.usgs.gov/modis/mod12q1v4.asp>). To sample natural variability in biophysical parameters of broadleaf forests resulting from the variations in climatic conditions and mixture of species, we selected for the analysis MODIS data subsets covering deciduous broadleaf forests of the eastern part of North America (MODIS tiles h11v04 and h12v04) and evergreen broadleaf forests of Amazonia (tile h12v09).

III. ANOMALIES IN THE MODIS LAI PRODUCT

An annual course of LAI and quality control (QC) data for the broadleaf forests pixels in the tiles h12v04 and h12v09 is shown in Fig. 2. The QC data indicate the proportion of pixels processed by different execution branches of the algorithm: the main algorithm with or without saturation (best quality), the backup algorithm (poor quality), and fill value. Overall, the backup algorithm retrievals are dominant during the winter and summer time for the tile h12v04. Retrievals for the tile h12v09 demonstrate less seasonality; however, most of retrievals are performed by the backup algorithm.

The anomalies in the MODIS LAI product both for herbaceous and woody vegetation have a single major source of explanation in terms of LUTs of the LAI algorithm. For a conceptual understanding of the source of anomalies, consider LAI retrievals from LAI–NDVI relationship as shown in Fig. 3. NDVI increases with increasing LAI until it reaches its maximum value at LAI ~ 3.5 and weakly depends on LAI thereafter (saturation domain). The retrieval anomalies were caused by the fact that MODIS LAI algorithm underestimated the upper limit of MODIS NDVI both for herbaceous and woody vegetation. In the case of herbaceous vegetation, typical LAI is low, and observed typical NDVI should not reach saturation domain. However, the MODIS LAI algorithm underestimated saturated NDVI, and the portion of observed high NDVI values reached modeled maximum NDVI, which resulted in LAI overestimation (Fig. 3). In the case of broadleaf forests, typical LAI and NDVI are high, and retrievals should be performed at saturation domain. However, observed NDVI values were substantially higher than modeled maximum NDVI, resulting in a failure of the main algorithm (Fig. 3).

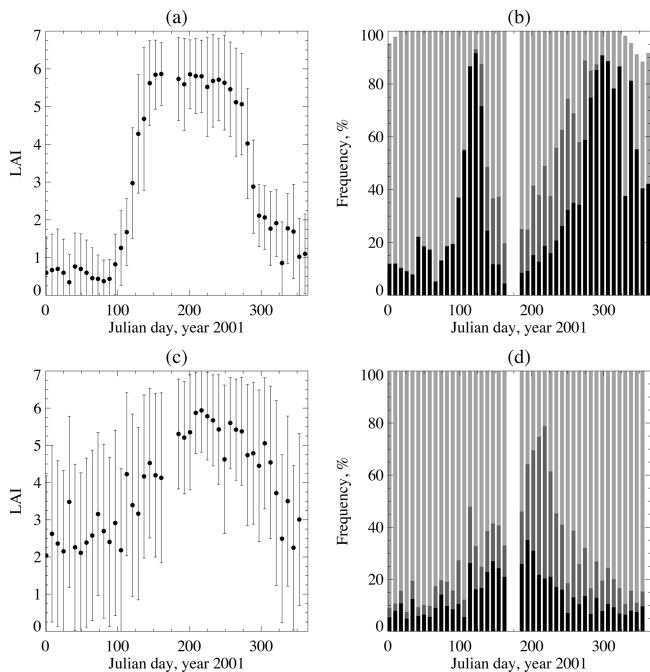


Fig. 2. Seasonal variations in LAI retrievals over deciduous broadleaf forests of the eastern part of North America (MODIS tile h12v04) and the evergreen broadleaf forest of Amazonia (MODIS tile h12v09). Panel (a) shows the annual course of the mean LAI and its standard deviation for tile h12v04 in year 2001, while panel (b) shows the annual course of the corresponding product Quality Control (QC)—the percentage of the main algorithm retrievals without saturation (black), the main algorithm retrievals with saturation (dark gray), the backup algorithm retrievals (light gray), and fill values (white). Panels (c) and (d) show the same but for tile h12v09.

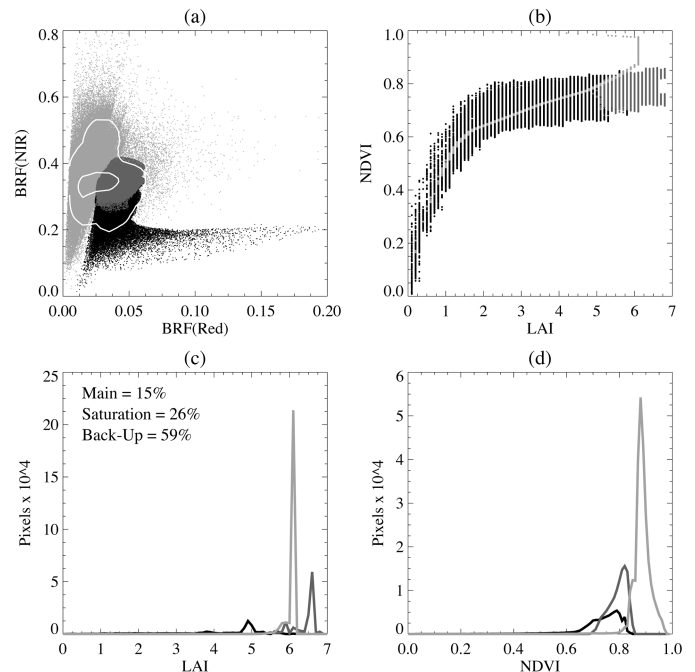


Fig. 4. LAI retrievals with Collection 4 LUTs and Collection 4 MODIS surface reflectances data over deciduous broadleaf forests in tile h12v04, Julian days 201–208 (July 20–27) in year 2001. Panel (a) shows partitioning of red–NIR spectral space by different execution branches of the LAI algorithm as well as contour plots of the overall data density. Panel (b) shows LAI–NDVI relationships, panel (c) LAI histograms, and panel (d) NDVI histograms for different execution branches. The grayscale coding of the execution branches is the same as in Fig. 2.

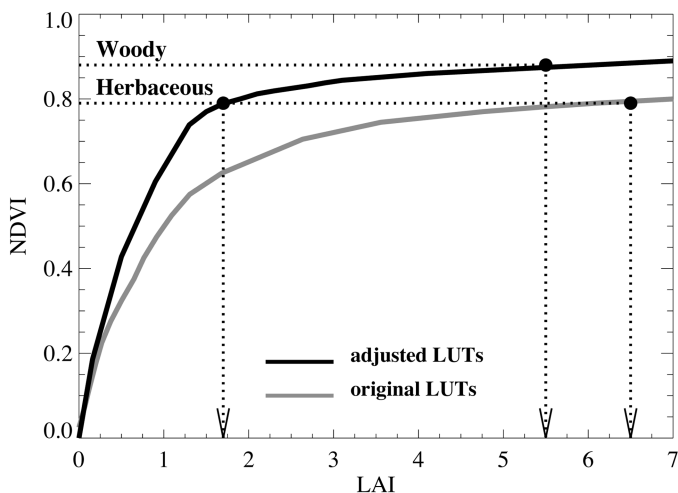


Fig. 3. Modeling the LAI–NDVI relationship for conceptual understanding of the anomalies in the LAI retrievals. NDVI at high LAI (> 3.5) reaches a saturation value, which is biome specific. If the saturated NDVI is underestimated, the retrievals over herbaceous vegetation (biomes 1–4) will result in unphysical peaks at high LAI values, or the failure of the algorithm in the case of woody vegetation (biomes 5–6).

Therefore, optimization of LAI retrievals requires increasing modeled maximum NDVI under condition of saturation. Note, however, that the main algorithm performs LAI retrievals not from NDVI but directly from MODIS channel data, which we analyze next.

Fig. 4 shows the analysis of LAI retrievals as a function of input surface reflectance data for the compositing period during

Julian days 201–208 (July 20–27) in year 2001, broadleaf forests pixels in the tile h12v04. Fig. 4(a) shows the distribution of reflectances in the red–NIR spectral space processed by different execution branches of the algorithm and overlaid with the contour plots of the highest density of surface reflectances. The retrieval domain of the main algorithm has a low degree of overlapping with MODIS observations, especially at low red reflectances, which caused a failure of the main algorithm. Next, consider the LAI–NDVI relationship derived from surface reflectances and LAI products, as shown in Fig. 4(b). Retrievals by the main algorithm without saturation are performed at low LAI values ($LAI < 3.5$), while retrievals by the main algorithm with saturation are concentrated at high LAI values. Also note the scatter of retrievals along the NDVI axis: this is due to the impact of soil patterns and view/illumination geometry. The LAI–NDVI curve generated by the backup algorithm is generally consistent with the main algorithm retrievals for low and medium NDVI. Range of high NDVI (0.82–1.0) is beyond of retrieval domain of the main algorithm; the backup algorithm performs retrievals, but reports a single LAI value of 6.1 [Fig. 4(c)–(d)]. The discussion in the following sections will detail the physics of LAI retrievals and provide guidelines for the changes to the LUTs to resolve the retrieval anomaly over broadleaf forests.

IV. PHYSICS OF THE MODIS LAI ALGORITHM

The retrieval technique of the MODIS LAI main algorithm is as follows. Given sun ($\vec{\Omega}_0$) and view ($\vec{\Omega}$) directions, bidirectional reflectance factor (BRF) at N_λ spectral bands, λ ,

band uncertainties, $\delta(\lambda)$, and six-biome land cover type, LC, find LAI. The BRF is defined as the ratio of the reflected flux from the surface area in a particular direction to the reflected flux from an ideal Lambertian surface [15]. The algorithm compares observed $[\text{BRF}^{\text{obs}}(\lambda, \text{LAI}, \vec{\Omega}, \vec{\Omega}_0)]$ and modeled $[\text{BRF}^{\text{mdl}}(\lambda, \text{LAI}, \vec{\Omega}, \vec{\Omega}_0)]$ BRFs for a suite of canopy structures and soil patterns that represent an expected range of typical conditions for a given biome type [12], [13]. All canopy/soil patterns for which modeled and observed BRFs differ within a specified uncertainties level, i.e., as shown at the bottom of the page, are considered as acceptable solutions. The mean values of LAI averaged over all acceptable solutions are reported as the output of the algorithm. Currently, only red and NIR MODIS channel data are utilized in LAI retrievals. When the main algorithm fails, the backup algorithm based on empirical LAI–NDVI relationships performs retrievals regardless of BRDF effect (dependence of BRF on view/illumination conditions) and uncertainties of surface reflectances for any nonfill value input. In view of atmospheric effects (cloud and aerosol contamination) and other environmental effects, the backup algorithm generally generates unreliable estimates of LAI.

The physical principles of BRF modeling by the main algorithm are illustrated in Fig. 5, which shows scatter plot of typical MODIS surface reflectances in the red–NIR spectral space for broadleaf forests during the growing season. The data grayscale coding corresponds to retrieval domains of execution branches of the algorithm. Also shown, are RT model predictions of BRF as function of LAI and soil reflectance. As LAI of vegetation canopy increases against an invariant background, the corresponding surface reflectance moves along the trajectories (soil isolines) in the spectral space away from the initial state specified by soil reflectance (Fig. 5) [4]. Independently from the background reflectances, the LAI trajectories converge to a common limiting point in the spectral space, when the leaf area tends to infinity. This situation is called the saturation domain and generally takes place for $\text{LAI} \gtrsim 3.5$. The location of the limiting point is mostly defined by the leaf spectral albedo (single-scattering albedo) and the view/illumination geometry. Accuracy of LAI retrievals at condition of saturation is highly sensitive to the precision of surface reflectances: small variations in surface reflectances result in high variation of LAI. Also, consider the shape of the retrieval domain of the main algorithm (Fig. 5). The range of soil reflectances in the LUTs of the algorithm is restricted to low values, which effectively allows cloud screening at high red and NIR reflectances near the soil line.

Next, we review the mathematical basis underlying structure of the LUTs of the MODIS LAI algorithm [12], [13]. The solution of the RT equation for a vegetation medium is constructed from the solution of two subproblems with the simplified boundary conditions: 1) black soil (BS) problem: the original illumination condition at the top of the canopy and the soil assumed to be absolutely absorbing; 2) soil (S) problem: there

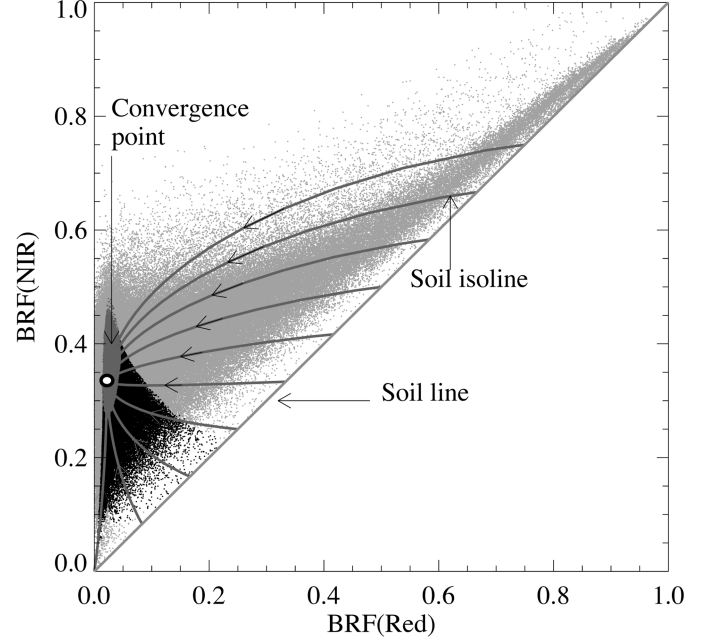


Fig. 5. Physical principles of BRF modeling by the MODIS LAI algorithm. The scatter plot of typical MODIS surface reflectances in the red–NIR spectral space for deciduous broadleaf forests during the growing season is shown. The grayscale coding corresponds to the retrieval domains of different execution branches of the MODIS LAI algorithm (refer to Fig. 2 for the scheme). Also shown are the model predictions of BRF as function of LAI. The stochastic RT model [23] was used in simulations with the following set of input parameters: $\omega(\text{red}) = 0.12$, $\omega(\text{NIR}) = 0.84$, $\text{SZA} = 30^\circ$, $\text{VZA} = 4^\circ$, $\text{RA} = 160^\circ$.

is no input energy from above, but a Lambertian energy source is located at the bottom of the canopy. Given the solutions of S- and BS-problems, the solution of the complete problem is constructed as follows:

$$\begin{aligned} \text{BRF}(\lambda, \text{LAI}, \vec{\Omega}, \vec{\Omega}_0) = & \text{BRF}_{\text{BS}}(\lambda, \text{LAI}, \vec{\Omega}, \vec{\Omega}_0) \\ & + \frac{\rho_{\text{soil}}(\lambda)}{1 - \rho_{\text{soil}}(\lambda) \cdot \text{DHR}_{\text{S}}(\lambda, \text{LAI})} \\ & \cdot T_{\text{BS}}(\lambda, \text{LAI}, \vec{\Omega}_0) \cdot \text{BRF}_{\text{S}}(\lambda, \text{LAI}, \vec{\Omega}) \end{aligned} \quad (1)$$

where BRF, BRF_{BS} , and BRF_{S} are the BRF of the complete problem, the BS-, and the S-problem, respectively, ρ_{soil} is the soil hemispherical reflectance, T_{BS} is the transmittance for BS-problem, and DHR_{S} is the DHR for the S-problem. Later in the text we use subscript “ x ” to denote subproblem ($x = \text{S}$ or BS). The DHR, directional-hemispherical reflectance is the ratio of the flux for light reflected by a surface area into a hemisphere to the illumination flux, when the target is illuminated with a parallel beam of light from a single direction [15]. Note that the parameterization of the LUTs in terms of the S- and the BS-problem allows for explicit parameterization of the influence of soil reflectance on the BRF of the complete problem and also simplify numerical solution of RT equation.

$$\frac{1}{N_\lambda} \cdot \sum_\lambda \left| \frac{\text{BRF}^{\text{obs}}(\lambda, \text{LAI}, \vec{\Omega}, \vec{\Omega}_0, \text{LC}) - \text{BRF}^{\text{mdl}}(\lambda, \text{LAI}, \vec{\Omega}, \vec{\Omega}_0, \text{LC})}{\delta(\lambda)} \right|^2 < 1$$

The solution of the x -problem is parameterized in terms of canopy absorptance A_x , transmittance T_x , and an anisotropy factor W_x , which is the ratio of BRDF to DHR. Absorptance and transmittance are stored only for the reference wavelength λ_0 to reduce the size of the LUTs. Absorptance and transmittance at an arbitrary wavelength are calculated for the x -problem according to the following approximation rules:

$$A_x(\lambda, \text{LAI}) = \frac{1 - \omega(\lambda_0) \cdot P_x^a(\text{LAI})}{1 - \omega(\lambda) \cdot P_x^a(\text{LAI})} \cdot \frac{1 - \omega(\lambda)}{1 - \omega(\lambda_0)} \cdot A_x(\lambda_0, \text{LAI}) \quad (2)$$

$$T_x(\lambda, \text{LAI}) = \frac{1 - \omega(\lambda_0) \cdot P_x^t(\text{LAI})}{1 - \omega(\lambda) \cdot P_x^t(\text{LAI})} \cdot T_x(\lambda_0, \text{LAI}) \quad (3)$$

where $\omega(\lambda)$ is the single-scattering albedo at wavelength λ , $\omega(\lambda_0)$ is the single-scattering albedo at a reference wavelength λ_0 . P_x^a and P_x^t are spectral invariants, which describe structure of vegetation canopy and can be derived from the radiative transfer equation [13], [24]. Given the absorptance and transmittance, and constrained by the energy conservation law, BRDF for both subproblems is calculated according to (4) and (5) as follows:

$$\text{DHR}_x(\lambda, \text{LAI}) = 1 - A_x(\lambda, \text{LAI}) - T_x(\lambda, \text{LAI}) \quad (4)$$

$$\text{BRF}_x(\lambda, \text{LAI}, \vec{\Omega}) = W_x(\lambda, \text{LAI}, \vec{\Omega}) \cdot \text{DHR}_x(\lambda, \text{LAI}). \quad (5)$$

To summarize, the LUTs of the main algorithm for broadleaf forests store the following set of parameters: 1) single-scattering albedo at the reference wavelength and at the red and NIR wavelengths; 2) absorptance and transmittance for the two subproblems at the reference wavelength; 3) spectral invariants for absorptance and transmittance for the two subproblems; 4) anisotropy factors for the two subproblems; 5) soil patterns at red and NIR wavelengths. Additionally, the LUTs for the backup algorithm (LAI-NDVI relationship) are generated based on the corresponding mean relationships, derived from the LUTs of the main algorithm.

V. OPTIMIZATION OF THE LUTS

The analysis of the Collection 4 LAI product for broadleaf forests indicates that Collection 4 LUTs are limited to simulate variability of MODIS surface reflectance data, which results in the failure of the main algorithm during growing season. To resolve this anomaly, we implemented modifications to the LUTs of the algorithm according to the following strategy: 1) simulated BRDFs should better overlap with typical MODIS surface reflectances in the red-NIR spectral space; 2) split broadleaf forests land cover class into deciduous and evergreen subclasses and develop separate LUTs for each subclass to better account for variability of the corresponding BRDFs; 3) the improved model simulations should result in the increase of the main algorithm retrievals with saturation for the typical case of high LAI values (3.5–7.0) of broadleaf forests; 4) the LAI values retrieved by the main algorithm should match field observations.

The Collection 5 LUTs were generated based on the stochastic RT model [23]. This model is based on the stochastic RT equations, derived by averaging standard three-dimensional (3-D) RT equation. Solution of the stochastic RT equation is a

mean radiation over horizontal plane, which is directly comparable with the pixel's average surface reflectance measured by MODIS. Stochastic one-dimensional (1-D) RT equations hold statistical information about 3-D spatial heterogeneity of vegetation in terms of probability of finding vegetation elements at particular depth and spatial-angular correlation matrix of the vegetation elements. The formulation of the model fully complies with the parameterization of the LUTs of the MODIS LAI algorithm (items 1–5 at the end of Section IV). Stochastic equations were solved numerically using method of successive orders of scattering approximations. Performance of the stochastic model was assessed with other 1-D and 3-D RT models, Monte Carlo model and field measurements [23]. The model has been utilized for multiple applications recently [11], [14], [24], [25], [35] and has better numeric stability, especially at the case of high LAI values and extreme view/illumination conditions, compared to the 3-D model, which has been used to generate previous versions of the LUTs. We want to emphasize that both models were developed based on similar physical principles and new model simulations should be considered as refinement to better describe features of MODIS data. The set of parameters of the stochastic RT model used to generate the new (Collection 5) LUTs is as follows. Single-scattering albedo at red and NIR wavelengths for deciduous (evergreen) broadleaf forests: $\omega(\text{red}) = 0.14$ ($= 0.12$), and $\omega(\text{NIR}) = 0.84$ ($= 0.74$). Reference single-scattering albedo was selected at the red wavelength, $\omega(\lambda_0) = \omega(\text{red})$. We selected 16 soil patterns for the deciduous broadleaf forests, and 5 for evergreen broadleaf forests. Soil reflectance starts from 0.01 with uniform step of 0.01 both at the red and NIR bands. The set of view/illumination conditions was specified as follows: solar zenith angle, $\text{SZA} = \{15^\circ, 30^\circ, 45^\circ, 60^\circ\}$, view zenith angle, $\text{VZA} = \{4^\circ, 15^\circ, 30^\circ, 45^\circ, 60^\circ\}$, relative azimuth, $\text{RA} = \{10^\circ, 40^\circ, 70^\circ, 100^\circ, 130^\circ, 160^\circ\}$. LAI was selected in the range $\{0.1-6.85\}$ with a step of 0.25. Uncertainties for the red and NIR bands were set to 30% and 15%, respectively, both for deciduous and evergreen broadleaf forests.

Figs. 6 and 7 compare sets of key variables generated with the Collection 4 and Collection 5 LUTs. BRDF simulated with the Collection 4 LUTs has a deficiency of nonmonotonic decrease of red and NIR reflectances at high LAI values due to the numerical errors and approximations used in (2) and (3) to calculate absorptance and transmittance [Fig. 6(a)]. The above errors were corrected in the Collection 5 LUTs [Fig. 6(b)]. Fig. 7(a)–(d) compares BRDFs simulated with the Collection 4 and Collection 5 LUTs at red and NIR wavelengths as function of LAI. Note that BRDFs were grouped by SZA, while the other parameters (VZA, RA, soil reflectance, and LAI) are varying within the constraints of LUTs. As SZA increases, the range of variations in BRDF increases for the same range of variation of VZA and RA, especially for the NIR. What changes in the parameters of the BS- and the S-problems result in the change of BRDF, described above? Fig. 6(c) and (d) shows the scatter plots of simulated BRDFs for both subproblems in the red-NIR spectral space. BRDF for BS-problem provides a major contribution to the total BRDF at high LAI values, because the impact of the soil reflectance is negligible in this case. Therefore, a nonmonotonic behavior of total BRDF at high LAI values in Collection 4 was due to the errors in BRDF for

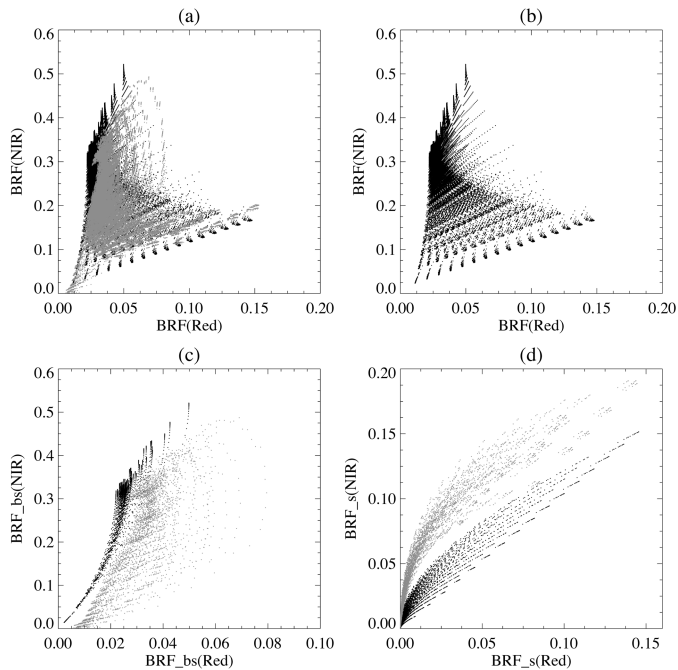


Fig. 6. Distribution in the red-NIR spectral space of total BRF [panels (a) and (b)] and BRFs for the S-problem [panel (c)] and the BS-problem [panel (d)] simulated with the Collection 4 (gray) LUTs for broadleaf forests class and Collection 5 (black) LUTs for deciduous broadleaf forests subclass.

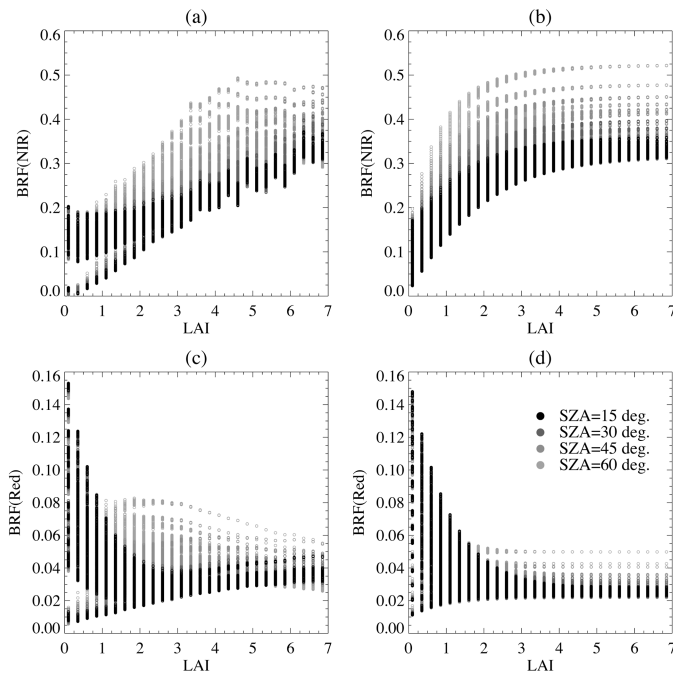


Fig. 7. BRF as function of LAI at red and NIR wavelengths, simulated with the Collection 4 [panels (a) and (c)] LUTs for broadleaf forests class and the Collection 5 [panels (b) and (d)] LUTs for deciduous broadleaf forests subclass. BRFs are grouped by solar zenith angle (SA = 15°, 30°, 45°, 60°), while the other parameters (view zenith angle, relative azimuth, soil reflectance, and LAI) are varying within the constraints of LUTs.

BS-problem. Also, the mean value and the range of variations of BRF for BS-problem at the red wavelength were decreased. Modifications to BRF for S-problem are minor: the general structure remained the same, however, the mean value of NIR reflectance decreased, especially for high LAI values.

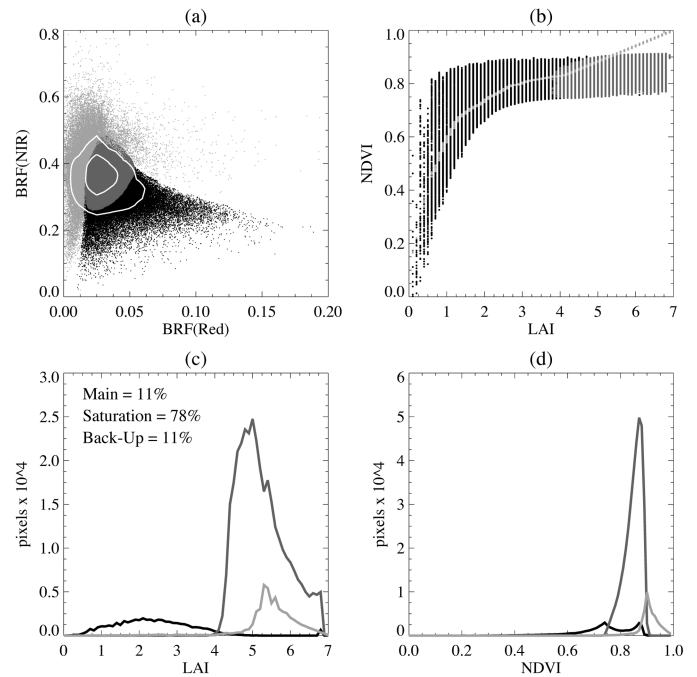


Fig. 8. LAI retrievals with the Collection 5 LUTs and the Collection 4 MODIS surface reflectances data over deciduous broadleaf forests in tile h12v04, Julian days 201–208 (July 20–27) in year 2001. Panel (a) shows partitioning of the red-NIR spectral space by different execution branches of the LAI algorithm as well as the contour plots of the overall data density. Panel (b) shows LAI-NDVI relationships, panel (c) LAI histograms, and panel (d) NDVI histograms for different execution branches. The grayscale coding of the execution branches is the same as in Fig. 2.

VI. EVALUATION OF THE OPTIMIZED RETRIEVALS WITH FIELD DATA

The analysis of LAI retrievals with the Collection 5 LUTs is presented in Fig. 8 for tile h12v04, deciduous broadleaf forests only, Julian days 201–208 (July 20–27) in year 2001. Compare the new results with the retrievals based on the Collection 4 LUTs (Fig. 4). The highest data density of MODIS surface reflectances closely matches the retrieval domain of the main algorithm with saturation. The portion of main algorithm retrievals with the Collection 5 LUTs was substantially increased: the main algorithm without saturation, 11% (versus 15% in Collection 4); the main algorithm with saturation, 78% (versus 26%); the backup algorithm, 11% (versus 59%).

Next, compare Collection 5, Collection 4 retrievals and the corresponding field measurements over two deciduous broadleaf forest sites in North America (Fig. 9) and one evergreen broadleaf forest site in Amazonia (Fig. 10). The BigFoot team (<http://www.fsl.orst.edu/larse/bigfoot/index.html>) [6] performed measurements during Julian day 201 (July 20) in year 2001 at 7 × 7 km area of the Harvard Forest FLUXNET site (center: latitude = 42.528 513°, longitude = -72.172 907°, MODIS tile h12v04, sample = 817, line = 896). Mean field LAI scaled to MODIS resolution was about 4.9 ± 0.8. The Collection 5 LAI averaged over the growing season is about 5.2, which agrees well with field measurements compared to Collection 4 retrievals (LAI ~ 6.0) [Fig. 9(a)]. Also note that the Collection 5 resolved the Collection 4 problem of LAI overestimation during winter season (LAI < 1 for Collection 5 versus LAI of 2–3 for Collection 4). Additionally, retrieval

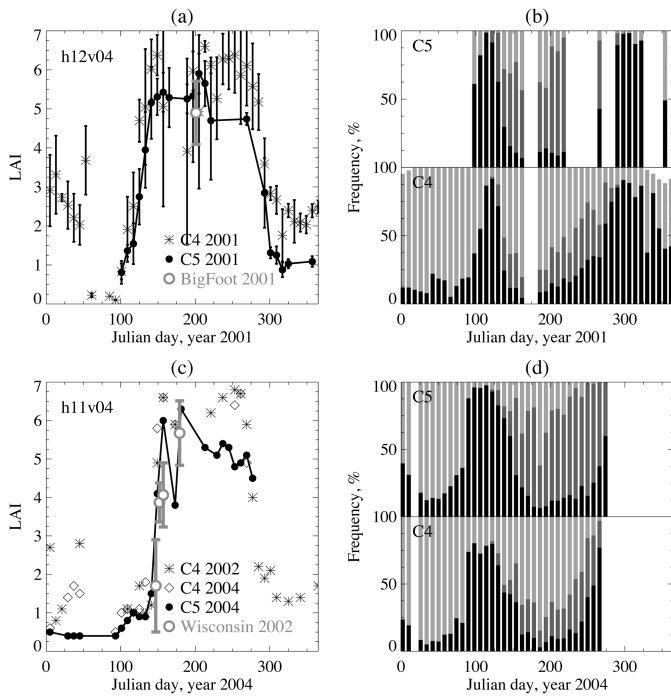


Fig. 9. Comparison of the Collection 4 and the Collection 5 MODIS LAI products with field measurements over deciduous broadleaf forests. Field data over 7×7 km area at the Harvard Forest FLUXNET site (latitude = 42.528513° , longitude = -72.172907° , MODIS tile h12v04, line = 896, sample = 817) were collected by Cohen *et al.* [6]. Field data over 540×540 m grid at the northern Wisconsin site (latitude = 45.804167° , longitude = -90.079853° , MODIS tile h11v04, line = 503, sample = 864) were collected by Ahl *et al.* [1]. Panel (a) shows annual course of MODIS LAI product averaged over 7×7 km site area and corresponding field measurements for Harvard Forest site, while panel (b) compares annual course of the Collection 4 and Collection 5 MODIS LAI QC for all broadleaf forests pixels in the tile h12v04. Panels (c) and (d) show the same but for Wisconsin site and tile h11v04. Grayscale coding of QC is the same as in Fig. 2.

rate of the main algorithm was increased by $> 30\%$ during the growing season at the scale of tile h12v04 [Fig. 9(b)].

Ahl *et al.* [1] measured spring green-up leaf phenology for a deciduous broadleaf forest during Julian day 147 (May 26), 152 (June 1), 157 (June 6), and 179 (June 28) in year 2002 at 540×540 m grid of the northern Wisconsin site (latitude = 45.804167° , longitude = -90.079853° , MODIS tile h11v04, line = 503, sample = 864). The Collection 5 LAI product was generated for year 2004, due to limited availability of MODIS data. The Collection 5 LAI and mean field LAI for the above dates are as follows: 1.5 (1.7 ± 1.2), 4.1 (3.9 ± 0.5), 6.0 (4.1 ± 0.8), and 6.3 (5.7 ± 0.8) [Fig. 9(c)]. Similarly to Harvard Forest site, LAI during winter time over Wisconsin site was decreased from about 2 to < 0.5 . The retrieval rate of the main algorithm was increased by $> 40\%$ during the growing season at the scale of tile h11v04 [Fig. 9(d)]. The small nonzero LAI values during the winter are likely due to the presence of evergreen samplings in the understory.

Measurements over evergreen broadleaf forests in Amazonia were performed by three teams. The BigFoot team performed measurements during Julian day 57 (February 26) in year 2002 at 7×7 km area of Tapajos FLUXNET site (center latitude = -2.869745° , longitude = -54.94355° , MODIS tile h12v09, line = 344, sample = 614). Huete *et al.* (personal communication) performed measurements during Julian day 185 (July 3) in

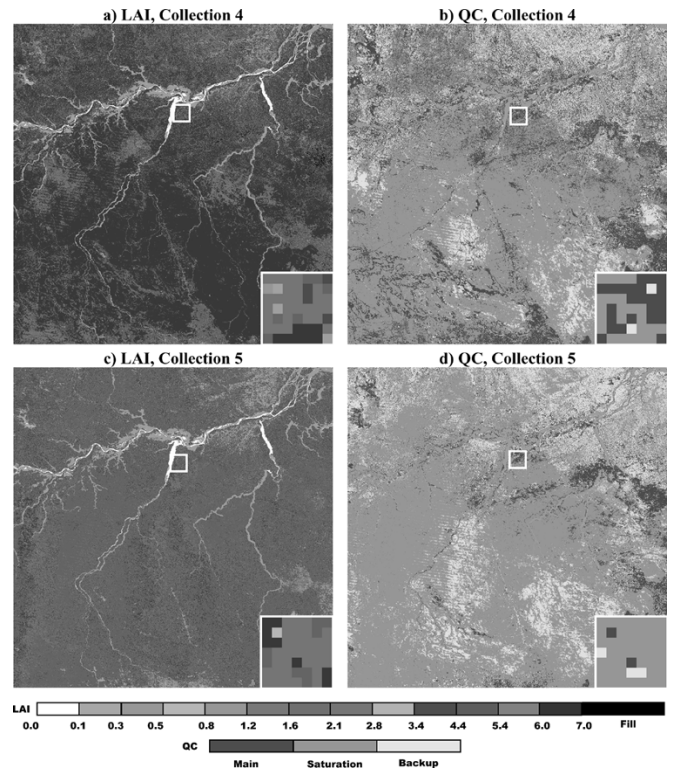


Fig. 10. Comparison of the Collection 4 and the Collection 5 LAI retrievals over evergreen broadleaf forests in Amazonia, MODIS tile h12v09, Julian days 201–208 (July 20–27) in year 2003. Panels (a) and (b) show, respectively, the Collection 4 LAI and QC. Panels (c) and (d) show the same but for the Collection 5. Bottom right inserts at each panel show 7×7 km subsets over Tapajos FLUXNET site (latitude = -2.869745° , longitude = -54.94355° , MODIS tile h12v09, line = 344, sample = 614).

year 2000 at several 250-m transects near the KM67 tower of the same site (latitude = -2.856667° , longitude = -54.958889° , MODIS tile h12v09, line = 342, sample = 613). Aragão *et al.* [2] performed large-scale transects during July 2001 over the area of Tapajos National Forest ($13\,000\text{ km}^2$, UL latitude = -2.75° /longitude = -55.50° , LR = -4.00° /longitude = -54.90°) which includes the above Tapajos site. For comparisons purposes we presented in Fig. 10 Collection 4 and Collection 5 LAI and QC data for tile h12v09, as well as corresponding subsets over 7×7 km area of Tapajos site for Julian days 201–208 in year 2003 (data for other years were not available). The Collections 5 and 4 mean LAI over the site area is 5.6 ± 0.9 and 5.2 ± 1.4 . Field measurements by BigFoot and Huete *et al.* indicate mean LAI of about 5.4–7.0 and 5.8–6.7, respectively. Mean LAI from Aragão *et al.* at the site is about 4. Comparison of LAI measurements by Aragão *et al.* and the Collections 4 and 5 MODIS products at the larger scale of Tapajos National Forest show that, on average, the Collection 5 MODIS LAI is higher than reference by about 2. This difference is of the order of disagreement between field data at the Tapajos site. Disagreement between field measurements could be due to the differences in the scale of observations and experimental design (plots against transects). Further large-scale LAI measurements at Amazonia by independent teams are required to reduce uncertainties of field measurements at dense forests.

In general, according to global surveys [3] average LAI over deciduous broadleaf forests is 5.1 ± 1.6 , and average LAI over

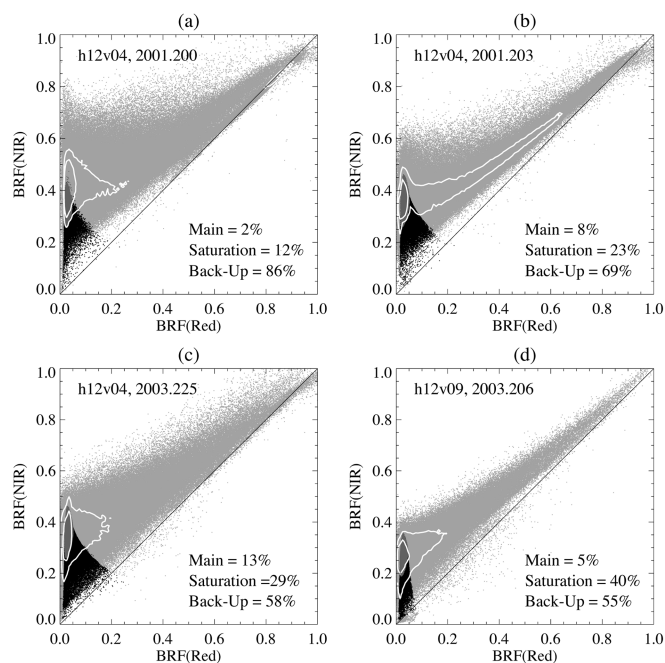


Fig. 11. Daily variations in the MODIS surface reflectances data over broadleaf forests in the red-NIR spectral space. Surface reflectances for Julian days 200 (July 19) and 203 (July 22) in year 2001, day 206 (July 25) in year 2003, all for deciduous broadleaf forest pixels in the tile h12v04 and day 225 (August 13) in year 2003 for evergreen broadleaf forest pixels in the tile h12v09 are compared in panels (a)–(d). Each plot shows the partitioning of surface reflectances in the red-NIR spectral space by different execution branches of the Collection 5 LAI algorithm as well as the contour plots of the data density. The grayscale coding of the execution branches is the same as in Fig. 2.

evergreen broadleaf forests is 5.7 ± 2.4 , which is in close agreement with the Collection 5 LAI product. Based on the analysis of the Collection 4 and 5 MODIS LAI products and comparison with available field measurements, we conclude that the requirements 1–4 for the LUTs optimization, specified in Section V, were satisfied.

VII. ANALYSIS OF VARIATIONS IN SURFACE REFLECTANCES AND LAI

A. Analysis of Daily LAI Retrievals

What factors in the physics of the LAI algorithm or the input data determine the accuracy of LAI retrievals? Consider Figs. 11 and 12, which compare the daily variations of MODIS surface reflectances for Julian day 200 (July 19) and 203 (July 22) in year 2001, day 225 (August 13) in year 2003, all for the tile h12v04 and day 206 (July 25) in year 2003 for tile h12v09. Fig. 11(a)–(d) shows the scatter plots of the MODIS surface reflectances in the red-NIR spectral space, processed by different execution branches of the algorithm. Each plot was overlaid with the contour plot of the data density. Fig. 12(a)–(d) and Table I show, respectively, histograms and most probable values of red, NIR, SZA, and VZA for the above datasets. One major factor that restricts accuracy of LAI retrievals is cloud contamination of the MODIS daily data. The presence of clouds is clearly indicated by the high data density located near the soil line at high red and NIR reflectances (Fig. 11). Cloud reflectances are beyond the retrieval domain of the main algorithm and, therefore, cause the failure of the main algorithm.

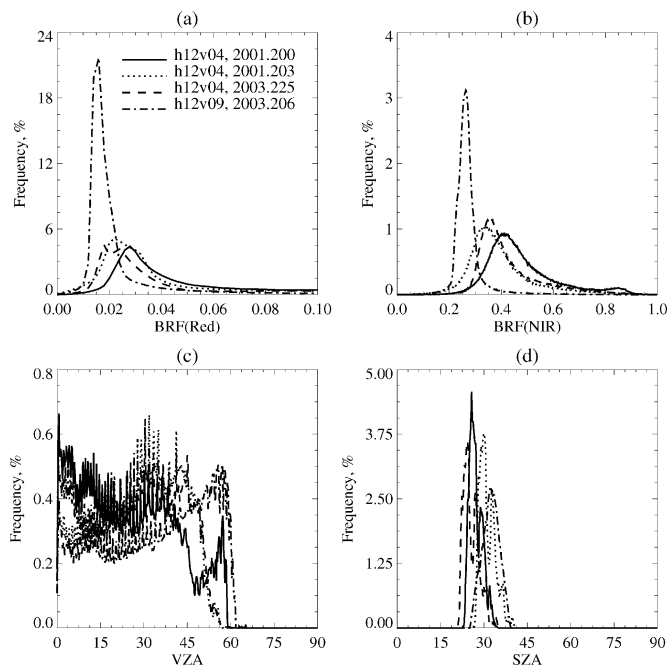


Fig. 12. Variations in the distributions of BRF at red and NIR wavelengths, VZA, and SZA are shown in panels (a)–(d) for the same dates/locations as in Fig. 11.

TABLE I
DAILY VARIATIONS IN SURFACE REFLECTANCE PARAMETERS (BRF AT RED AND NIR WAVELENGTHS, NDVI, AND SOLAR ZENITH ANGLE) FOR MODIS TILES h12v04 AND h12v09

Tile ID	Date	BRF(Red)	BRF(NIR)	NDVI	SZA
h12v04	2001.193	0.032	0.500	0.874	24.8
	2001.194	0.028	0.420	0.876	22.4
	2001.195	0.016	0.510	0.884	27.0
	2001.196	0.026	0.394	0.862	23.8
	2001.197	0.028	0.448	0.870	29.6
	2001.198	0.028	0.398	0.860	24.6
	2001.199	0.026	0.354	0.884	30.2
	2001.200	0.028	0.412	0.864	25.8
	2001.201	0.018	0.342	0.884	22.4
	2001.202	0.030	0.430	0.858	28.2
	2001.203	0.018	0.354	0.888	24.2
	2001.204	0.032	0.456	0.862	29.0
	2001.205	0.024	0.378	0.872	25.4
	2001.206	0.028	0.430	0.872	31.0
	2001.207	0.024	0.390	0.872	27.0
	2001.208	0.018	0.328	0.886	23.2
	2003.225	0.022	0.338	0.858	30.2
	2003.226	0.034	0.422	0.850	34.6
	2003.227	0.022	0.330	0.854	31.4
	2003.228	0.022	0.462	0.858	36.6
2003.229	0.026	0.376	0.860	33.0	
2003.230	0.020	0.308	0.868	29.8	
2003.231	0.030	0.376	0.850	34.0	
2003.232	0.020	0.310	0.868	31.8	
h12v09	2003.201	0.026	0.322	0.850	36.2
	2003.202	0.014	0.234	0.880	28.6
	2003.203	0.026	0.340	0.850	38.4
	2003.204	0.014	0.246	0.878	30.6
	2003.205	0.026	0.364	0.854	39.2
	2003.206	0.016	0.264	0.878	32.2
	2003.207	0.028	0.376	0.856	41.0
2003.208	0.016	0.274	0.860	34.8	

However, daily MODIS surface reflectances demonstrate significant variability over broadleaf forests, which is not due to clouds. Consider variations of surface reflectances for deciduous broadleaf forests in tile h12v04. Between July 19, 2001 and August 13, 2003 the most probable value of red varies from

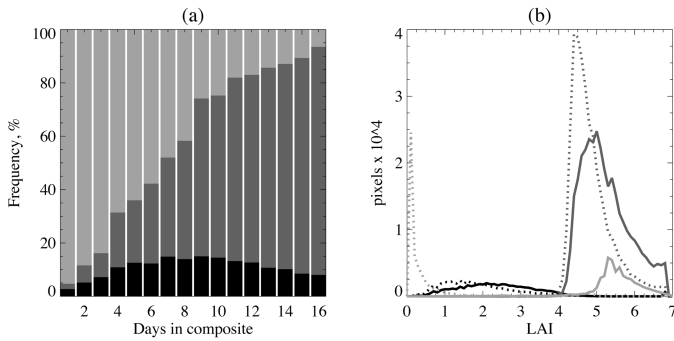


Fig. 13. Impact of the compositing of multiple MODIS observations on Collection 5 LAI retrievals. Panel (a) shows trends in the relative percentages of retrievals by the three execution branches of the LAI algorithm as function of the length of compositing period. Daily LAI data were generated by the LAI algorithm with Collection 5 LUTs for Julian days 193–208 (July 12–27) in year 2001, tile h12v04. Panel (b) shows variations in the distribution of LAI, retrieved by the three execution branches of the algorithm during Julian days 201–208 (July 20–27) in year 2001, tile h12v04. The solid lines correspond to the compositing option when the maximum LAI for the given execution branch was selected to represent the compositing value, while the dashed lines correspond to the minimum LAI option. The grayscale coding of the execution branches is the same as in Fig. 2.

0.028 to 0.022 (21% difference), and from 0.412 to 0.338 (18% difference) for NIR band (Table I). These variations are comparable to the algorithm's band uncertainties (Section V). Range of variations is significantly larger if we also take into account evergreen broadleaf forests. Most probable value of red and NIR reflectances is 0.016 and 0.264 for evergreen broadleaf forests in tile h12v09 during July 25, 2003 (Table I). The observed variability is not due to BRDF effect as distributions of SZA and VZA, shown in Fig. 12(c) and (d), are similar. Therefore, the observed variability should be due to a limited accuracy of atmospheric correction and the natural variability of surface reflectances for different species. The optimized algorithm addresses the last problem: broadleaf forests class was divided into deciduous and evergreen subclasses and subclass-specific LUTs were generated (cf. Section V). Note that geolocation errors coupled with adjacency effects (not studied here) also degrade precision of the MODIS data. Further increase of the accuracy of LAI retrievals requires extension of the set of remote sensing observations: 1) by increasing compositing length, and/or 2) by implementing multisensor retrievals (the combined MODIS Terra and Aqua product). We analyze the first option in the next section. Analysis of the combined product can be found in a separate publication [32].

B. Analysis of LAI Compositing

The compositing scheme of the MODIS LAI algorithm selects the LAI value during eight-day compositing period based on the best quality retrievals followed by maximum LAI. Compare the daily retrievals [Fig. 11(b)] and the corresponding composite [Fig. 8(a)]. Compositing provides cloud screening and accumulates MODIS observations, which fit to the LUTs of the main algorithm and reduce uncertainties inherited from the upstream products. In the analysis, we used daily and corresponding compositing data for Julian days 193–208 (July 12–27) in year 2001, deciduous broadleaf forests pixels in tile h12v04 (Fig. 13). Consider Fig. 13(a), which demonstrates rapid increase of the quality of the LAI retrievals from 5% for

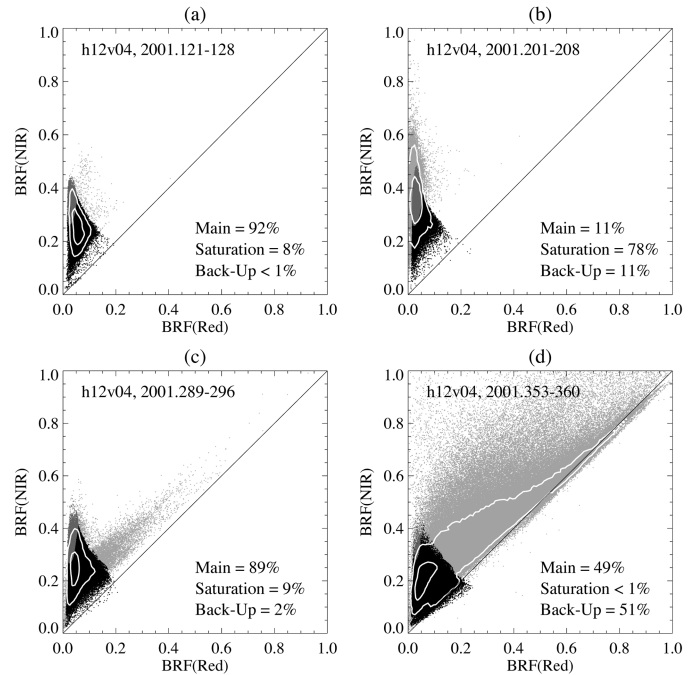


Fig. 14. Seasonal variations in the MODIS surface reflectances data over deciduous broadleaf forests in the red–NIR spectral space. Composites of surface reflectances for winter, spring, summer, and fall seasons corresponding to Julian days 121–128 (May 01–08), 201–208 (July 20–27), 289–296 (October 16–23), and 353–360 (December 19–26), all in year 2001, for deciduous broadleaf pixels in tile h12v04 are shown in panels (a)–(d). Each plot shows the partitioning of surface reflectances in the red–NIR spectral space by different execution branches of the Collection 5 LAI algorithm as well as the contour plots of the data density. The grayscale coding of the execution branches is the same as in Fig. 2.

a single day up to 58% for eight days and up to 94% for 16 days. The rate of increase in the quality of retrievals depends on the season and the geolocation: retrievals over regions with constant cloud cover or snow covered areas will be improved from extension of the compositing period. Next, consider the variability of daily LAI data during an eight-day compositing period for the main and backup algorithms. For analysis, we select the minimum LAI value generated by the same execution branch, which was used to generate maximum compositing value. The histograms of the minimum and the maximum LAI are shown in Fig. 13(b). The retrievals by the main algorithm show low variability between the maximum and the minimum values. However, variations in LAI retrievals by the backup algorithm are large (0.2–5.5), which indicates the low reliability of the backup retrievals due to cloud contamination and the general uncertainties of surface reflectances. On average, the compositing scheme for main algorithm selects between 1.1 days out of eight compositing days to generate a composite LAI, while the compositing scheme for the backup algorithm selects between 7.9 days. Overall, extension of compositing period helps to increase retrieval rate of the main algorithm and reduce noise in the product, given that: 1) MODIS and simulated surface reflectances are consistent, and 2) phenological changes during compositing period are not significant.

C. Analysis of Seasonality in LAI and Surface Reflectances

What changes in MODIS surface reflectances result in the observed seasonality in LAI retrievals over deciduous broadleaf

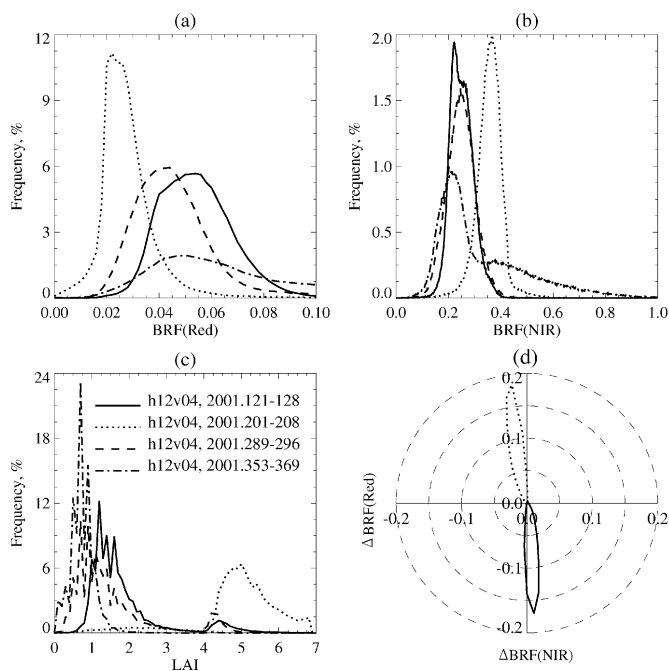


Fig. 15. Variations in the distributions of BRF at red and NIR wavelengths, and LAI are shown in panels (a)–(c) for the same dates/location as in Fig. 14. The polar plot in panel (d) shows the distribution of changes in red and NIR surface reflectances due to the phenological changes in vegetation properties during the transition from (dotted line) spring to summer and (solid line) from summer to fall.

TABLE II

SEASONAL VARIATIONS OF SURFACE REFLECTANCE PARAMETERS (BRF AT RED AND NIR WAVELENGTHS, NDVI, AND SOLAR ZENITH ANGLE) AND LAI RETRIEVALS (LAI AND QUALITY CONTROL FLAGS) FOR MODIS TILE h12v04. ABBREVIATIONS USED FOR QUALITY CONTROL FLAGS ARE AS FOLLOWS: “M” IS FOR THE MAIN ALGORITHM WITHOUT SATURATION, “S” IS FOR THE MAIN ALGORITHM WITH SATURATION, AND “B” IS FOR THE BACKUP ALGORITHM RETRIEVALS

Date	BRF (Red)	BRF (NIR)	NDVI	SZA	LAI	M/S/B
2001.097	0.076	0.224	0.44	37.0	1.0 ± 0.3	61 0 39
2001.105	0.076	0.224	0.45	35.4	1.0 ± 0.4	82 0 18
2001.113	0.070	0.226	0.54	32.8	1.2 ± 0.4	99 0 1
2001.121	0.056	0.222	0.65	31.2	1.8 ± 1.0	92 8 0
2001.129	0.030	0.294	0.84	23.4	3.0 ± 1.5	63 36 1
2001.137	0.030	0.326	0.83	25.4	3.7 ± 1.5	30 42 28
2001.145	0.032	0.346	0.86	23.8	4.5 ± 1.3	16 53 31
2001.153	0.028	0.350	0.88	23.0	4.8 ± 1.2	11 66 23
2001.185	0.026	0.354	0.89	26.6	4.6 ± 1.5	11 51 38
2001.193	0.026	0.354	0.87	25.6	4.5 ± 1.6	14 44 42
2001.201	0.020	0.352	0.89	23.8	4.9 ± 1.2	11 78 11
2001.209	0.026	0.350	0.87	26.4	5.0 ± 1.1	9 76 15
2001.217	0.024	0.350	0.87	27.0	4.8 ± 1.1	11 84 5
2001.265	0.028	0.308	0.84	45.2	3.5 ± 1.5	43 50 7
2001.289	0.044	0.246	0.70	53.8	1.5 ± 1.1	89 9 2
2001.297	0.050	0.188	0.61	60.4	0.9 ± 0.4	98 0 2
2001.305	0.050	0.214	0.62	62.4	0.9 ± 0.3	98 0 2
2001.313	0.054	0.196	0.58	60.8	0.8 ± 0.3	90 0 10
2001.321	0.058	0.216	0.59	64.0	0.9 ± 0.3	93 0 7
2001.353	0.050	0.220	0.54	69.8	0.8 ± 0.4	49 0 51

forests? Composites of surface reflectances and LAI for spring, summer, fall, and winter seasons corresponding to Julian days 121–128 (May 01–08), 201–208 (July 20–27), 289–296 (October 16–23), and 353–360 (December 19–26), all in year 2001, deciduous broadleaf pixels in tile h12v04 were compared (Figs. 14 and 15). Note the changes in LAI and corresponding changes in the location of predominant data density of surface

reflectances from the location near the soil line toward the limiting point (the saturation domain) during the transition from spring to summer and back-ward from summer to fall. Note also the wide range of variation of surface reflectance along the soil line during winter time due to the dominance of bare background (dark surface reflectances), clouds and snow (bright reflectances). Even the eight-day compositing was not able to remove snow and clouds effects due to the persistence of such conditions. Additional details on seasonality in surface reflectances and LAI retrievals can be found in Table II.

VIII. CONCLUSION

The analysis of the Collection 4 MODIS LAI product for broadleaf forests indicates that the Collection 4 LUTs of the algorithm are limited to simulate variability of MODIS surface reflectance data, which results in the failure of the main algorithm during growing season and disagreement with field measurements. LAI retrievals over dense vegetation (broadleaf forests during the growing season) are mostly performed over a compact location in the spectral space of saturated surface reflectances, which need to be accurately modeled to be consistent with remote sensing observations. The saturated surface reflectances are mostly sensitive to leaf albedo and view/illumination geometries. The new LUTs were generated with the stochastic RT model, parameters of which were selected to model majority of MODIS data during seasonal cycle and to provide higher accuracy simulations at high LAI values and extreme view/illumination conditions. Separate LUTs were developed for deciduous and evergreen broadleaf forests. Daily variations of surface reflectances over global broadleaf forests, caused by a limited accuracy of atmospheric correction and natural variability of surface reflectances for different species and land cover mixtures, set a limit for retrieval improvements. Further increase in the accuracy of the MODIS LAI product requires extension of the set of the input remote sensing observations. This can be achieved by extending the compositing period or alternatively by utilizing data from several sensors (the combined MODIS Terra and Aqua LAI product).

ACKNOWLEDGMENT

The authors appreciate the contribution of the BigFoot team for validation of the MODIS land products.

REFERENCES

- [1] D. E. Ahl, S. T. Gower, and S. N. Burrows, “Monitoring spring canopy phenology of a deciduous broadleaf forest using MODIS,” *Remote Sens. Environ.*, to be published.
- [2] L. E. O. C. Aragão, Y. E. Shimabukuro, F. D. B. E. Santo, and M. Williams, “Spatial validation of collection 4 MODIS LAI product in Eastern Amazon,” *IEEE Trans. Geosci. Remote Sens.*, 2005, to be published.
- [3] G. P. Asner, J. M. O. Scurlock, and J. A. Hicke, “Global synthesis of leaf area index observations: Implications for ecological and remote sensing studies,” *Global Ecol. Biogeograph.*, vol. 12, pp. 191–205, 2003.
- [4] F. Baret, S. Jacquemoud, and J. F. Hanocq, “The soil line concept in remote sensing,” *Remote Sens. Rev.*, vol. 7, pp. 65–82, 1993.
- [5] G. B. Bonan, K. W. Oleson, M. Vertenstein, S. Levis, X. Zeng, Y. Dai, R. Dickinson, and Z. L. Yang, “The land surface climatology of the community land model coupled to the NCAR community climate model,” *J. Clim.*, vol. 15, pp. 3123–3149, 2002.

- [6] W. B. Cohen, T. K. Maier-sperger, Z. Yang, S. T. Gower, D. P. Turner, W. D. Ritts, M. Berterretche, and S. W. Running, "Comparisons of land cover and LAI estimates derived from ETM+ and MODIS for four sites in North America: A quality assessment of 2000/2001 provisional MODIS products," *Remote Sens. Environ.*, vol. 88, pp. 233–255, 2003.
- [7] R. E. Dickinson, A. Henderson-Sellers, P. J. Kennedy, and M. F. Wilson, "Biosphere-Atmosphere Transfer Scheme (BATS) for the NCAR CCM," NCAR Res., Boulder, CO, NCAR/TN-275-STR, 1986.
- [8] M. A. Friedl, D. K. McIver, J. C. F. Hodges, X. Y. Zhang, D. Muchoney, A. H. Strahler, C. E. Woodcock, S. Gopal, A. Schneider, and A. Cooper, "Global land cover mapping from MODIS: Algorithms and early results," *Remote Sens. Environ.*, vol. 83, pp. 287–302, 2002.
- [9] D. Huang, B. Tan, W. Yang, N. V. Shabanov, Y. Knyazikhin, and R. B. Myneni, "Precision and accuracy of the MODIS LAI as a function of errors in input upstream products," In preparation.
- [10] C. O. Justice, J. R. G. Townshend, E. F. Vermote, E. Masuoka, R. E. Wolfe, N. Saleous, D. P. Roy, and J. T. Morisette, "An overview of MODIS land data processing and product status," *Remote Sens. Environ.*, vol. 83, pp. 3–15, 2002.
- [11] R. K. Kaufmann, L. Zhou, Y. Knyazikhin, N. V. Shabanov, R. B. Myneni, and C. J. Tucker, "Effect of orbital drift and sensor changes on the time series of AVHRR vegetation index data," *IEEE Trans. Geosci. Remote Sens.*, vol. 38, no. 6, pp. 2584–2597, Nov. 2000.
- [12] Y. Knyazikhin, J. V. Martonchik, R. B. Myneni, D. J. Diner, and S. Running, "Synergistic algorithm for estimating vegetation canopy leaf area index and fraction of absorbed photosynthetically active radiation from MODIS and MISR data," *J. Geophys. Res.*, vol. 103, pp. 32 257–32 275, 1998.
- [13] Y. Knyazikhin, J. V. Martonchik, D. J. Diner, R. B. Myneni, M. Verstraete, B. Pinty, and N. Gorbon, "Estimation of vegetation canopy leaf area index and fraction of absorbed photosynthetically active radiation from atmosphere-corrected MISR data," *J. Geophys. Res.*, vol. 103, pp. 32 239–32 256, 1998.
- [14] S. Kotchenova, N. V. Shabanov, Y. Knyazikhin, A. B. Davis, R. Dubayah, and R. B. Myneni, "Modeling lidar waveforms with time-dependent stochastic radiative transfer theory for remote estimates of forest structure," *J. Geophys. Res.*, vol. 108, no. D15, p. 4484, 2003.
- [15] J. V. Martonchik, C. J. Bruegge, and A. H. Strahler, "A review of reflectance nomenclature used in remote sensing," *Remote Sens. Rev.*, vol. 19, pp. 9–20, 2000.
- [16] J. M. Melillo, A. D. McGuire, D. W. Kicklighter, B. Moore, C. J. Vorostmaty, and A. L. Schloss, "Global climate change and terrestrial net primary productivity," *Nature*, vol. 363, pp. 234–240, 1993.
- [17] J. T. Morisette, J. L. Privette, and C. O. Justice, "A framework for the validation of MODIS land products," *Remote Sens. Environ.*, vol. 83, pp. 77–96, 2002.
- [18] R. B. Myneni, S. Hoffman, Y. Knyazikhin, J. L. Privette, J. Glassy, Y. Tian, Y. Wang, X. Song, Y. Zhang, G. R. Smith, A. Lotsch, M. Friedl, J. T. Morisette, P. Votava, R. R. Nemani, and S. W. Running, "Global products of vegetation leaf area and fraction absorbed PAR from year one of MODIS data," *Remote Sens. Environ.*, vol. 83, pp. 214–231, 2002.
- [19] C. S. Potter, J. T. Randerson, C. B. Field, P. A. Matson, P. M. Vitousek, H. A. Mooney, and S. A. Klooster, "Terrestrial ecosystem production: A process model based on global satellite and surface data," *Global Biogeochem. Cycles*, vol. 7, no. 4, pp. 811–841, 1993.
- [20] J. L. Privette, R. B. Myneni, Y. Knyazikhin, M. Mukufute, G. Roberts, Y. Tian, Y. Wang, and S. G. Leblanc, "Early spatial and temporal validation of MODIS LAI product in Africa," *Remote Sens. Environ.*, vol. 83, pp. 232–243, 2002.
- [21] S. W. Running and J. C. Coughlan, "A general model of forest ecosystem processes for regional applications," *Ecol. Model.*, vol. 42, pp. 124–154, 1988.
- [22] P. J. Sellers, D. A. Randall, G. J. Collatz, J. A. Berry, C. B. Field, D. A. Dazlich, C. Zhang, G. D. Collelo, and L. Bounoua, "A revised land surface parameterization (SIB2) for atmospheric GCM's. Part I: Model formulation," *J. Clim.*, vol. 9, pp. 676–705, 1996.
- [23] N. V. Shabanov, Y. Knyazikhin, F. Baret, and R. B. Myneni, "Stochastic modeling of radiation regime in discontinuous vegetation canopies," *Remote Sens. Environ.*, vol. 74, no. 1, pp. 125–144, 2000.
- [24] N. V. Shabanov, Y. Wang, W. Buermann, J. Dong, S. Hoffman, G. Smith, Y. Tian, Y. Knyazikhin, and R. B. Myneni, "Effect of foliage spatial heterogeneity in the MODIS LAI and FPAR algorithm over broadleaf forests," *Remote Sens. Environ.*, vol. 85, no. 4, pp. 410–423, 2003.
- [25] N. V. Shabanov, L. Zhou, Y. Knyazikhin, C. J. Tucker, and R. B. Myneni, "Analysis of interannual changes in northern vegetation activity observed in AVHRR data during 1981 to 1994," *IEEE Trans. Geosci. Remote Sens.*, vol. 40, no. 1, pp. 115–130, Jan. 2002.
- [26] B. Tan, D. Huang, J. Hu, W. Yang, P. Zhang, N. V. Shabanov, Y. Knyazikhin, and R. B. Myneni, "Assessment of the broadleaf crops leaf area index product from the Terra MODIS instrument," *Agricult. Forest Meteorol.*, Jan. 2005, submitted for publication.
- [27] B. Tan, J. Hu, P. Zhang, D. Huang, N. V. Shabanov, M. Weiss, Y. Knyazikhin, and R. B. Myneni, "Validation of Moderate Resolution Imaging Spectroradiometer leaf area index product in croplands of Alpiilles, France," *J. Geophys. Res.—Atmos.*, vol. 110(D01), no. 107, 2005. DOI: 10.1029/2004JD004860.
- [28] Y. Tian, Y. Zhang, Y. Knyazikhin, R. B. Myneni, J. M. Glassy, G. Dedieu, and S. W. Running, "Prototyping of MODIS LAI and FPAR algorithm with LASUR and LANDSAT data," *IEEE Trans. Geosci. Remote Sens.*, vol. 38, no. 5, pp. 2387–2401, Sep. 2000.
- [29] E. F. Vermote, N. Z. El Saleous, C. O. Justice, Y. J. Kaufman, J. L. Privette, L. Remer, J. C. Roger, and D. Tanre, "Atmospheric correction of visible to middle-infrared EOS-MODIS data over land surfaces: Background, operational algorithm and validation," *J. Geophys. Res.—Atmos.*, vol. 102, no. D14, pp. 17 131–17 141, 1997.
- [30] Y. Wang, Y. Tian, Y. Zhang, N. Z. El-Saleous, Y. Knyazikhin, E. F. Vermote, and R. B. Myneni, "Investigation of product accuracy as a function of input and model uncertainties: Case study with SeaWiFS and MODIS LAI/FPAR algorithm," *Remote Sens. Environ.*, vol. 78, pp. 299–313, 2001.
- [31] Y. Wang, C. E. Woodcock, W. Buermann, P. Stenberg, P. Voipio, H. Smolander, T. Hame, Y. Tian, J. Hu, Y. Knyazikhin, and R. B. Myneni, "Evaluation of the MODIS LAI algorithm at a coniferous forest site in Finland," *Remote Sens. Environ.*, vol. 91, pp. 114–127.
- [32] W. Yang, N. V. Shabanov, D. Huang, R. E. Dickinson, R. R. Nemani, Y. Knyazikhin, and R. B. Myneni, "Analysis of prototype Collection 5 products of leaf area index from Terra and Aqua MODIS sensors," *J. Geophys. Res.*, 2005, to be published.
- [33] W. Yang, J. C. Stroeve, N. V. Shabanov, D. Huang, B. Tan, P. Zhang, Y. Knyazikhin, and R. B. Myneni, "Analysis of leaf area index and fraction absorbed PAR products from the Terra MODIS sensor: 2000–2004," *IEEE Trans. Geosci. Remote Sens.*, 2005, to be published.
- [34] W. Yang, B. Tan, D. Huang, M. Rautiainen, N. V. Shabanov, Y. Wang, J. L. Privette, K. F. Huemmerich, R. Fensholt, I. Sandholt, M. Weiss, D. E. Ahl, S. T. Gower, R. R. Nemani, Y. Knyazikhin, and R. B. Myneni, "MODIS leaf area index products: From validation to algorithm improvement," *IEEE Trans. Geosci. Remote Sens.*, 2005, to be published.
- [35] Y. Zhang, N. V. Shabanov, Y. Knyazikhin, and R. B. Myneni, "Assessing information content of multiangle satellite data for mapping biomes. II Theory," *Remote Sens. Environ.*, vol. 80, pp. 1–12, 2001.
- [36] Y. Zhang, Y. Tian, Y. Knyazikhin, J. V. Martonchik, D. J. Diner, M. Leroy, and R. B. Myneni, "Prototyping of MISR LAI and FPAR algorithm with POLDER data over Africa," *IEEE Trans. Geosci. Remote Sens.*, vol. 38, no. 5, pp. 2402–2418, Sep. 2000.

Authors' photographs and biographies not available at the time of publication.